Journal of Organometallic Chemistry 694 (2009) 2831–2838

Contents lists available at ScienceDirect

Journal of Organometallic Chemistry

journal homepage: www.elsevier.com/locate/jorganchem

# Density functional theory study of the mechanism for $Ni(NHC)_2$ catalyzed dehydrogenation of ammonia–borane for chemical hydrogen storage

Xinzheng Yang, Michael B. Hall *

*Department of Chemistry, Texas A&M University, College Station, Texas 77843-3255, United States*

ARTICLE INFO

*Article history:*
Received 4 February 2009
Received in revised form 15 April 2009
Accepted 16 April 2009
Available online 3 May 2009

*Keywords:*
Chemical hydrogen storage
Ammonia–borane
Catalytic mechanism
N-heterocyclic carbene nickel
Density functional theory

ABSTRACT

The mechanism for catalytic dehydrogenation of ammonia–borane (AB = $H_3N–BH_3$), a promising candidate for chemical hydrogen storage, by the $Ni(NHC)_2$ complexes was studied by using density functional theory at the non-empirical meta-GGA level, Tao–Perdew–Staroverov–Scuseria (TPSS) functional, with all-electron correlation-consistent polarized valence double-zeta (cc-pVDZ) basis set. The mechanism for both the first and the second $H_2$ release from AB was studied for the first time. Several unusual aspects of this catalytic mechanism were revealed through our calculations. First, the first $H_2$ release begins with proton transfer from nitrogen to the Ni bound carbene carbon, forming a new C–H bond, instead of the previously hypothesized direct B–H or N–H bond activation. Second, this new C–H bond is activated by the metal, transferring the H to Ni, then forming the $H_2$ molecule by transferring another H from B to Ni, rather than β-H transfer. Third, the second $H_2$ release from $H_2N–BH_2$ begins with the breaking of a 3-center, 2-electron Ni–H–B bridging structure with the assistance of the unsaturated carbene carbon atom to form a B–C bond. Fourth, a nearly rhombic $N_2B_2H_6$ structure is formed to help the regeneration of the catalyst $Ni(NHC)_2$. These reaction pathways explain the importance of NHC ligands in this catalytic process and yield lower energy barriers than those mechanisms that begin with N–H or B–H activations catalyzed by the metal atoms. The predicted reaction mechanism which features unexpected ligand participation points the way to finding new catalysts with higher efficiency, as partial unsaturation of the M–L bond may be essential for low energy H transfers.

© 2009 Elsevier B.V. All rights reserved.

## 1. Introduction

The acceleration of global climate change and the energy crisis caused by the wide use of fossil fuel has encouraged the development of hydrogen as a clean secondary energy source that can reduce the emission of greenhouse gases. One of the challenges in the development of the hydrogen economy is the storage of hydrogen with high reliability and safety, which requires for practical reasons, high density, low cost, and fast release rate. As a promising chemical hydrogen storage material both in its commercial availability and physical and chemical properties, ammonia–borane (AB = $H_3N–BH_3$) has attracted increasing attention in very recent years [1–22]. AB is a solid at room temperature, stable in air and water and contains 19.6 wt.% $H_2$, much higher than the target of US Department of Energy (DOE) for an on-board hydrogen storage system (9.0 wt.% H by 2015) [23]. Although neat AB can release more than 2 equiv. of $H_2$ by heating to modest temperature, its direct hydrogen release rate is too slow to be practical. Enhancing the release rate and ratio of hydrogen released from AB is one of the foremost challenges in its practical use. In this regard, transition metal catalyzed AB dehydrogenation reactions in solution have been examined both experimentally and computationally in recent years [11–22].

In a recently reported experimental study of transition metal catalyzed dehydrogenation of AB, Baker and coworkers [17] described a series of new catalysts based on N-heterocyclic carbene (NHC) nickel complexes, which are the best of few examples of active, low-cost, first-transition-row metal catalysts for the dehydrogenation of AB reported to date. Although these $Ni(NHC)_2$ complexes do not catalyze the fastest release rate of hydrogen, they extend the hydrogen release from AB to an unprecedented 18 wt.% for the first time with 20-fold increase in activity compared to the uncatalyzed reaction at the temperature of 60 °C. Lacking a detailed catalytic mechanism for the dehydrogenation of AB on $Ni(NHC)_2$, Baker and coworkers hypothesized a requisite mechanism, beginning with B–H bond activation through oxidative addition and then β-H elimination from a N–H bond, for the steps in the first cycle of AB dehydrogenation ($H_3N–BH_3 \rightarrow H_2N–BH_2 + H_2$). In our communication [20] of the first computational study of the catalytic mechanism for the first $H_2$ release from AB on the unsimplified experimental catalyst, 2,2′-bis(1,3,4-triphenyl-4,5-dihydro-1*H*-1,2,4-triazol-5-ylidene)-Ni, we found that

* Corresponding author. Tel.: +1 979 845 1843; fax: +1 979 845 2971.
*E-mail address:* mbhall@tamu.edu (M.B. Hall).

0022-328X/$ - see front matter © 2009 Elsevier B.V. All rights reserved.
doi:10.1016/j.jorganchem.2009.04.018

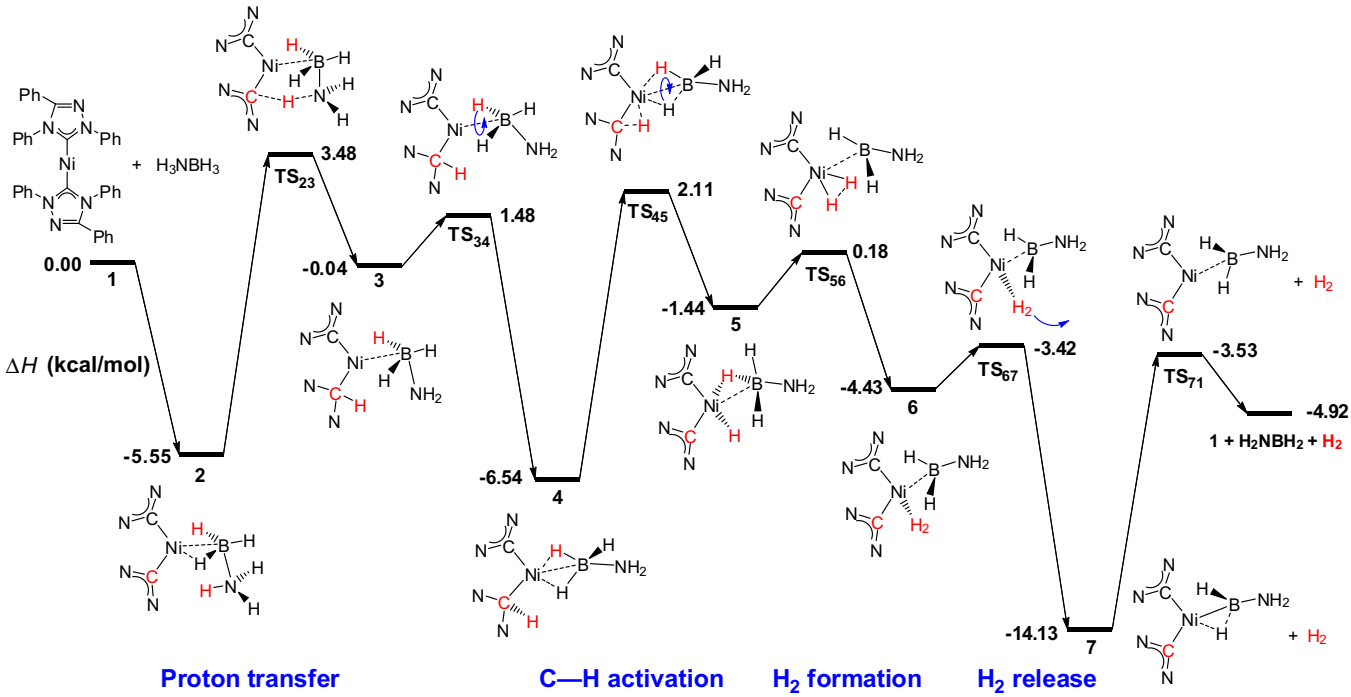


**Scheme 1.** Predicted reaction mechanism and gas-phase relative enthalpies of the first $H_2$ release from ammonia–borane catalyzed by $Ni(NHC)_2$ showing four main steps: (1) transfer of a proton from N to the unsaturated C in carbene, (2) transfer of H from this C to Ni, (3) transfer of H from B to Ni, and (4) release of $H_2$ and $H_2B–NH_2$ to regenerate the catalyst $Ni(NHC)_2$.

the first $H_2$ release from AB has four main steps: (1) transfer of a proton from N to the unsaturated C in carbene, (2) transfer of H from this C to Ni, (3) transfer of H from B to Ni, and (4) release of $H_2$ and $H_2B–NH_2$ to regenerate the catalyst $Ni(NHC)_2$ (Scheme 1). This mechanism explained the importance of the unsaturated NHC ligands in this catalytic reaction. In this full paper, the mechanism for the first equivalent of $H_2$ release from AB is discussed in more detail, including the evaluation of computational methods and the previously hypothesized mechanism. Furthermore, a very interesting mechanism for the second $H_2$ release from $H_2N–BH_2$ is shown to involve the unsaturated NHC ligand in B–C bond formation. To our knowledge, this is the first theoretical study of the catalytic mechanism for both the first and the second equivalent of $H_2$ release from AB.

**Table 1**
Relative electronic energies calculated by using different density functional for the rate determining steps: **2** → **TS$_{23}$**, **4** → **TS$_{45}$** and **7** → **TS$_{71}$**. The geometric structures are optimized by using TPSS. The energies of other functionals are calculated at these geometries.

| Density functional | Relative electronic energies (kcal/mol) | | |
|---|---|---|---|
| | $E^{\ddagger}$ (**TS$_{23}$**) − $E^{\circ}$ (**2**) | $E^{\ddagger}$ (**TS$_{45}$**) − $E^{\circ}$ (**4**) | $E^{\ddagger}$ (**TS$_{71}$**) − $E^{\circ}$ (**7**) |
| TPSS | 12.83 | 11.27 | 10.79 |
| TPSSh | 13.92 | 11.54 | 10.35 |
| PBE | 10.45 | 12.35 | 11.59 |
| PBE0 | 12.43 | 12.97 | 12.16 |
| B3LYP | 13.28 | 13.21 | 5.81 |
| B3PW91 | 12.25 | 12.53 | 9.86 |
| BMK | 13.55 | 14.25 | 10.99 |

## 2. Computational details

All calculations were performed using the density functional theory in the GAUSSIAN 03 suite of *ab initio* programs [24]. To evaluate the performance of DFT on this system, several different types of generalized gradient approximation (GGA) density functionals were examined for the relative electronic energies of the rate determining steps: **2** → **TS$_{23}$**, **4** → **TS$_{45}$** and **7** → **TS$_{71}$**. These density functionals include the straight GGA (PBE [25]), hybrid GGA (PBE0 [25], B3LYP [26,27] and B3PW91 [26,28]), meta-GGA (TPSS [29]) and hybrid meta-GGA (TPSSh [29] and BMK [30]). The basis sets used for all of these calculations are at the all-electron correlation-consistent polarized valence double-zeta [31] (cc-pVDZ) level (including 895 basis functions and 2254 primitive Gaussians for intermediate **2**). The geometric structures were optimized at TPSS/cc-pVDZ level and the energies of other functionals were calculated at these geometries. According to the results listed in Table 1, these density functionals produce very similar relative electronic energies for these key barriers except the result of the B3LYP calculation for **7** → **TS$_{71}$**. Therefore, since TPSS is the only non-empirical meta-GGA density functional among them and as it has a much higher computational efficiency than hybrid functionals, we chose TPSS for all the further calculations. Calculating the harmonic vibrational frequencies and noting the number of imaginary frequencies confirmed the nature of all intermediates (no imaginary frequency) and transition-state structures (only one imaginary frequency), which also were confirmed to connect reactants and products by the intrinsic reaction coordinate (IRC) calculations. The effect of solvent was taken into account by performing reaction field calculations using integral equation formalism polarizable continuum models (IEF-PCM) for benzene. The zero-point energy (ZPE) and entropic contribution have been estimated within the harmonic potential approximation. The enthalpies, $H$, and free energies, $G$, were calculated for $T = 298.15$ K. All relative enthalpies and free energies are reported in kcal/mol and based on the separated reagents $Ni(NHC)_2$ and $H_3N–BH_3$ are set equal to 0.0 kcal/mol. The molecular structure figures are drawn by using the JIMP2 molecular visualization and manipulation program [32].

## 3. Results and discussion

### 3.1. Catalytic mechanism for the first $H_2$ release from AB

Our predictions for the complete catalytic cycle of the first $H_2$ release from AB, including relative gas-phase enthalpies, are displayed in Scheme 1. Corresponding structures are drawn in Fig. 1. Calculated relative gas-phase enthalpies, gas-phase free energies and free energies in solvent (benzene) in the reaction pathway are listed in Table 1. At first, AB and the catalyst $Ni(NHC)_2$ bind directly to form a relatively stable intermediate **2**, in which AB links to Ni through the electrons in B–H bonds with one B–H–Ni interaction dominating. Our structure **2** does not involve a $\kappa^3$-$H_3B$–$NH_3$ interaction but has a geometry more typical of a H–X σ-complex [33]. From **2**, a hydrogen atom bound to the nitrogen of AB moves toward one NHC ligand and in particular the unsaturated carbon atom bonding with Ni, and forms a C–H bond through transition state $\mathbf{TS_{23}}$ with a gas-phase enthalpic barrier of only 9.03 kcal/mol ($\Delta G^{\ddagger}_{solv} = 11.94$ kcal/mol). In $\mathbf{TS_{23}}$, the H is migrating as a proton to the "$sp^2$" electron pair on the carbene, which rotates to donate this pair to the $H^+$ and to accept a pair of electrons from Ni formally oxidizing it to $Ni^{II}$, or alternatively a $Ni^0$ with a "reverse" metal-to-ligand dative bond [34]. The N lone pair created in this $H^+$ transfer begins the formation of the B–N multiple bond: shortening the B–N distance, lengthening a B–H bond, and shortening the corresponding Ni–H distance. Intermediate **3** is not very stable, and $H_2N$–$BH_3$ rotates about the Ni–B vector through a rather low energy transition state $\mathbf{TS_{34}}$ ($\Delta H^{\ddagger}$ = 1.44 kcal/mol) to form a more stable intermediate **4**. These movements convert the tetrahedral structure at Ni in **3** to the square-planar structure in **4**; shorten the B–N and two Ni–H bond lengths by about 0.1 Å; and lead to an increase in stability by 6.50 kcal/mol. As shown in Fig. 1, the C–Ni–B–N dihedral angles of **3**, $\mathbf{TS_{34}}$ and **4** are −16.17°, 12.37° and 87.80°, indicating the movement of the B–N bond.

Then, the hydrogen atom that has just detached from nitrogen and bonded to the carbon atom moves toward Ni through transition state $\mathbf{TS_{45}}$ with an enthalpic barrier of 8.65 kcal/mol ($\Delta G^{\ddagger}_{solv} = 7.90$ kcal/mol), and bonds to Ni forming intermediate **5**. Here, the transfer is formally $H^-$ and Ni remains formally $Ni^{II}$ in **5**. In addition to the formation of the Ni–H bond in **5**, the $H_2N$–$BH_3$ has rotated and one H has moved further from B to form a 3-center, 2-electron Ni–H–B bridging interaction. These two hydrogen atoms then move together through transition state $\mathbf{TS_{56}}$: breaking the B–H bond, creating the H–H bond, and forming intermediate **6** over a rather low enthalpic barrier ($\Delta H^{\ddagger}$ = 1.62 kcal/mol). Finally, $H_2$ is easily released to form intermediate **7**, which has shorter Ni–C, Ni–H and Ni–B bonds and is more stable than **6** by about 9.7 kcal/mol. Loss of $H_2N$–$BH_2$ first is somewhat less favorable. The catalyst $Ni(NHC)_2$ regenerates after release of $H_2N$–$BH_2$ through transition state $\mathbf{TS_{71}}$ ($\Delta H^{\ddagger}$ = 10.6 kcal/mol and $\Delta G^{\ddagger}_{solv} = 9.18$ kcal/mol).

According to the results listed in Table 2, the free energy differences of the rate determining steps $\mathbf{2} \rightarrow \mathbf{TS_{23}}$, $\mathbf{4} \rightarrow \mathbf{TS_{45}}$ and $\mathbf{7} \rightarrow \mathbf{TS_{71}}$, are 11.33, 8.56 and 8.52 kcal/mol in gas phase and 11.94, 7.90 and 9.18 kcal/mol in benzene solvent. Because of the entropic penalty, especially in solvent model, **2** has higher relative free energy than the separated $Ni(NHC)_2$ and AB.

### 3.2. Evaluation of the mechanisms beginning with B–H and N–H bond activations

In our effort to determine the most likely reaction pathway, we also calculated structures proposed by Baker and coworkers in their hypothesized catalytic mechanism, which begins with B–H bond activation through oxidative addition and then β-H elimination from a N–H bond for the first $H_2$ release from AB [17]. Although the transition state for the cleavage of the B–H bond in **2** activated by Ni was not found, we optimized the possible stable structure after the B–H bond cleavage, H–$Ni(NHC)_2(H_2BNH_3)$, which is displayed in Fig. 2. Its relative gas-phase enthalpy is already 6.8 kcal/mol higher than that of $\mathbf{TS_{23}}$, indicating that the AB dehydrogenation catalyzed by $Ni(NHC)_2$ cannot begin with B–H bond activation.

Besides the mechanism beginning with B–H bond activation, Luo et al. [18] proposed a mechanism beginning with N–H bond activation for the dehydrogenation of $Me_2NH$–$BH_3$ catalyzed by $Cp_2Ti$. Here, the corresponding mechanism beginning with Ni activated N–H bond cleavage was examined by optimizing the stable structure $(NHC)_2Ni$–$H_3NBH_3$ (Fig. 2) and the transition state $\mathbf{TS_{N-H-Ni}}$ (Fig. 2). $(NHC)_2Ni$–$H_3NBH_3$ is very close to **2** in energy. However, $\mathbf{TS_{N-H-Ni}}$ activates the N–H bond of the $(NHC)_2Ni$–$H_3NBH_3$ through an enthalpic barrier of 22.6 kcal/mol (gas phase). These results indicate that both B–H and N–H bond activations catalyzed directly by Ni have much higher energy barriers than proton transfer from N to carbene carbon ($\mathbf{2} \rightarrow \mathbf{TS_{23}}$).

### 3.3. Catalytic mechanism for the second $H_2$ release from AB

One of the most important properties of these $Ni(NHC)_2$ catalysts is that they can release up to 18 wt.% of $H_2$ from AB, which is more than 2 equiv. of $H_2$. This release of a second equivalent of $H_2$ allows this system to exceed the 2015 research target of DOE for an on-board hydrogen storage system. Therefore, understanding of the mechanism for the second $H_2$ release from AB is also very important. Based on the above study of the mechanism for the first $H_2$ release, a reaction pathway for the second $H_2$ release from AB has been calculated and is shown in Scheme 2. The calculated relative gas-phase enthalpies, gas-phase free energies and free energies in solvent (benzene) for this reaction pathway are listed in Table 3. Several important intermediate and transition-state structures in this reaction pathway are shown in Fig. 3.

Beginning from **7**, the "product" following the release of the first $H_2$, Ni and the unsaturated carbene carbon atom can again activate one of the 3-center, 2-electron Ni–H–B bridging bonds. As shown in the figure of transition state $\mathbf{TS_{78}}$ (Fig. 3), the mechanism is different in this case as B moves toward the unsaturated carbon atom while that H atom moves to the Ni, and forms intermediate **8** with a short Ni–H bond (1.53 Å) and a new B–C bond. The distance between Ni and the C bonding with B in **8** is 2.89 Å, indicating that one of the Ni–C bonds in the catalyst has been broken in this step. This is the rate determining step in this reaction pathway with an enthalpic barrier of 26.8 kcal/mol ($\mathbf{7} \rightarrow \mathbf{TS_{78}}$). This is much higher than the energy barriers for the first $H_2$ release and explains why this catalytic reaction needs higher temperature (60 °C) to release 18 wt.% of hydrogen from AB. We also explored the N–H activation of **7**, but the enthalpic barrier is 33.9 kcal/mol. In the next intermediate, **9**, a dihydrogen bound to Ni is formed from **8** through transition state $\mathbf{TS_{89}}$, in which a N–H bond is activated and this H atom moves from N to the hydrogen already bonding with Ni. Then, **9** can easily release this dihydrogen through transition state $\mathbf{TS_{9,10}}$ with a very low energy barrier and form intermediate **10**. By now, the second equivalent of $H_2$ has been released from AB. The following steps in this mechanism describe the regeneration of catalyst $Ni(NHC)_2$ and possible further reactions.

From **10**, the NHC group bonding with B moves back to Ni easily through transition state $\mathbf{TS_{10,11}}$ and regenerates the catalyst structure $Ni(NHC)_2$ with HN–BH bound through Ni–B and Ni–N bonds (intermediate **11**). Due to the strong Ni–B and Ni–N interactions (the calculated gas-phase enthalpy of binding for **1** and HN–BH is 25.3 kcal/mol), HN–BH cannot dissociate from $Ni(NHC)_2$ directly.

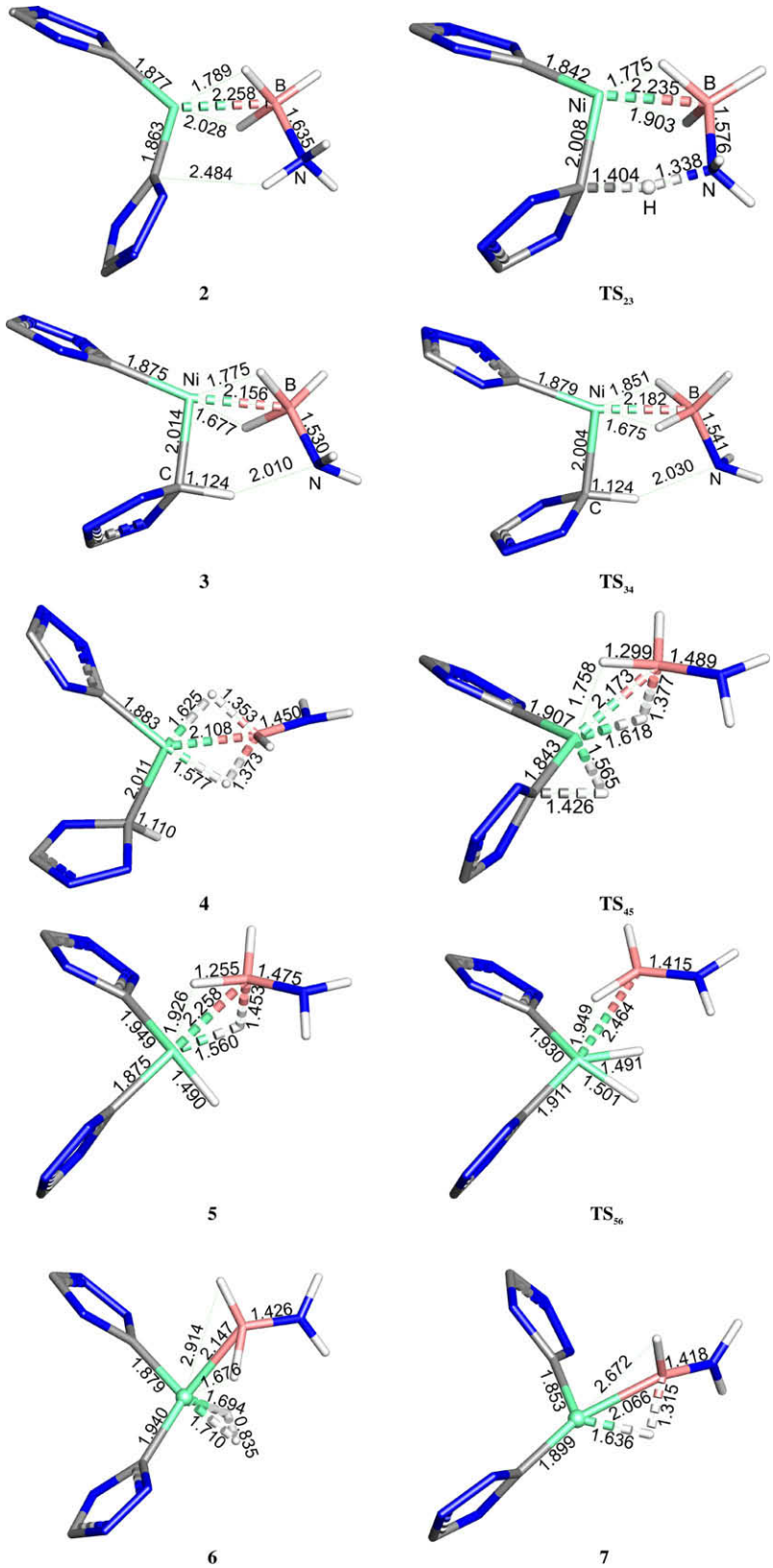


**Fig. 1.** Optimized geometric structures of complexes **2**, **3**, **4**, **5**, **6** and **7** and the transition states $\mathbf{TS_{23}}$ ($-1193.1\ cm^{-1}$), $\mathbf{TS_{34}}$ ($-85.3\ cm^{-1}$), $\mathbf{TS_{45}}$ ($-389.9\ cm^{-1}$) and $\mathbf{TS_{56}}$ ($-511.0\ cm^{-1}$). Bond lengths are in angstrom. The phenyl groups are not shown for clarity. The C–Ni–B–N dihedral angles of **3**, $\mathbf{TS_{34}}$ and **4** are −16.17°, 12.37° and 87.80°.

However, a previously released $H_2N–BH_2$ molecule from the first catalytic cycle can attach to the HN–BH structure in **11** easily through transition state $\mathbf{TS_{11,12}}$ simultaneously forming two N–B bond interactions and a very stable intermediate **12** (3.9 kcal/mol lower than **7**) with a nearly rhombic $N_2B_2H_6$ structure bonding to Ni. Then, as the N atom binding with Ni moves away from Ni, an-

**Table 2**
Calculated relative gas-phase enthalpies, gas-phase free energies and free energies in solvent (benzene) of the structures in the reaction pathway of the first $H_2$ release from ammonia–borane catalyzed by $Ni(NHC)_2$.

| Reaction steps | $\Delta H$ (gas) | $\Delta G$ (gas) | $\Delta G$ (solvent) |
|---|---|---|---|
| **1** | 0.00 | 0.00 | 0.00 |
| **2** | −5.55 | 8.62 | 16.48 |
| **$TS_{23}$** | 3.48 | 19.95 | 28.42 |
| **3** | −0.04 | 14.90 | 23.44 |
| **$TS_{34}$** | 1.48 | 18.80 | 27.38 |
| **4** | −6.54 | 8.55 | 16.99 |
| **$TS_{45}$** | 2.11 | 17.11 | 24.89 |
| **5** | −1.44 | 14.04 | 21.17 |
| **$TS_{56}$** | 0.18 | 13.83 | 22.89 |
| **6** | −4.43 | 10.58 | 19.36 |
| **$TS_{67}$** | −3.42 | 11.44 | 20.31 |
| **7** + $H_2$ | −14.13 | −8.59 | 0.41 |
| **$TS_{71}$** + $H_2$ | −3.53 | −0.07 | 9.59 |
| **1** + $H_2NBH_2$ + $H_2$ | −4.92 | −13.20 | −8.32 |

**Table 3**
Calculated relative gas-phase enthalpies, gas-phase free energies and free energies in solvent (benzene) of the structures in the reaction pathway of the second $H_2$ release.

| Reaction steps | $\Delta H$ (gas) | $\Delta G$ (gas) | $\Delta G$ (solvent) |
|---|---|---|---|
| **7** | −14.13 | −8.59 | 0.41 |
| **$TS_{78}$** | 12.67 | 19.66 | 28.56 |
| **8** | −6.61 | −0.16 | 8.28 |
| **$TS_{89}$** | 12.50 | 18.43 | 27.45 |
| **9** | 4.56 | 9.89 | 20.26 |
| **$TS_{9,10}$** | 5.46 | 11.04 | 24.76 |
| **10** | 3.09 | 1.52 | 12.41 |
| **$TS_{10,11}$** | 10.13 | 8.71 | 18.64 |
| **11** | 2.58 | 0.57 | 12.32 |
| **$TS_{11,12}$** | 12.44 | 20.46 | 28.85 |
| **12** | −18.01 | −6.08 | 0.63 |
| **$TS_{12,13}$** | −9.48 | 1.31 | 9.56 |
| **13** | −17.16 | −6.61 | 0.93 |
| **1** + $N_2B_2H_6$ | −5.77 | −9.67 | −7.41 |

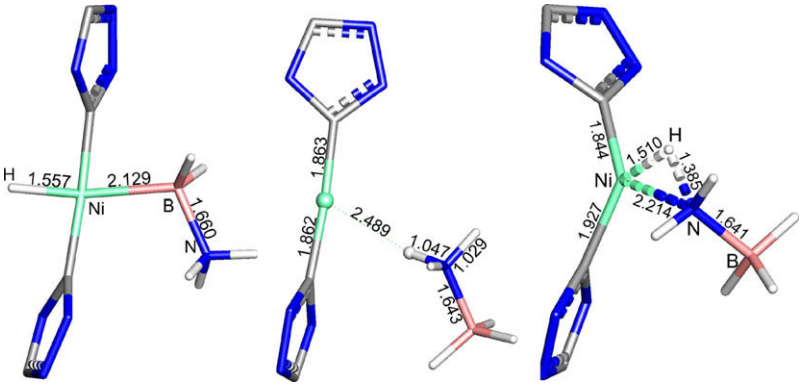


**Fig. 2.** The optimized stable structures of H–Ni(NHC)$_2$(H$_2$BNH$_3$) (left) after the B–H bond cleavage of intermediate **2** and (NHC)$_2$Ni–H$_3$NBH$_3$ (middle) and transition state **$TS_{N-H-Ni}$** (right, −935.5 cm$^{-1}$) for Ni activated N–H bond splitting. Bond lengths are in angstrom. The phenyl groups are not shown for clarity.

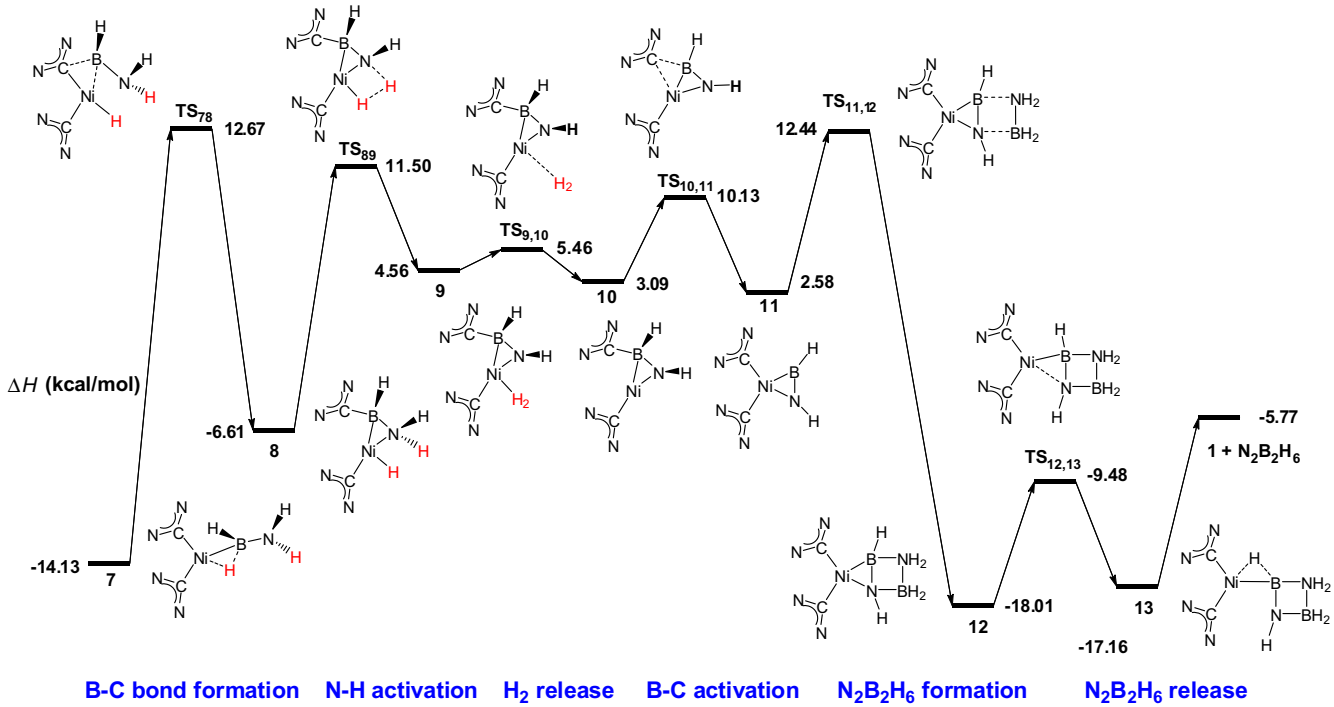


**Scheme 2.** Predicted reaction mechanism and relative gas-phase enthalpies of the second $H_2$ release from ammonia–borane catalyzed by $Ni(NHC)_2$ showing six main steps: (1) formation of B–C bond, (2) N–H bond activation for the formation of $H_2$, (3) $H_2$ release, (4) B–C bond activation, (5) $N_2B_2H_6$ formation and (6) $N_2B_2H_6$ release and regeneration of $Ni(NHC)_2$.

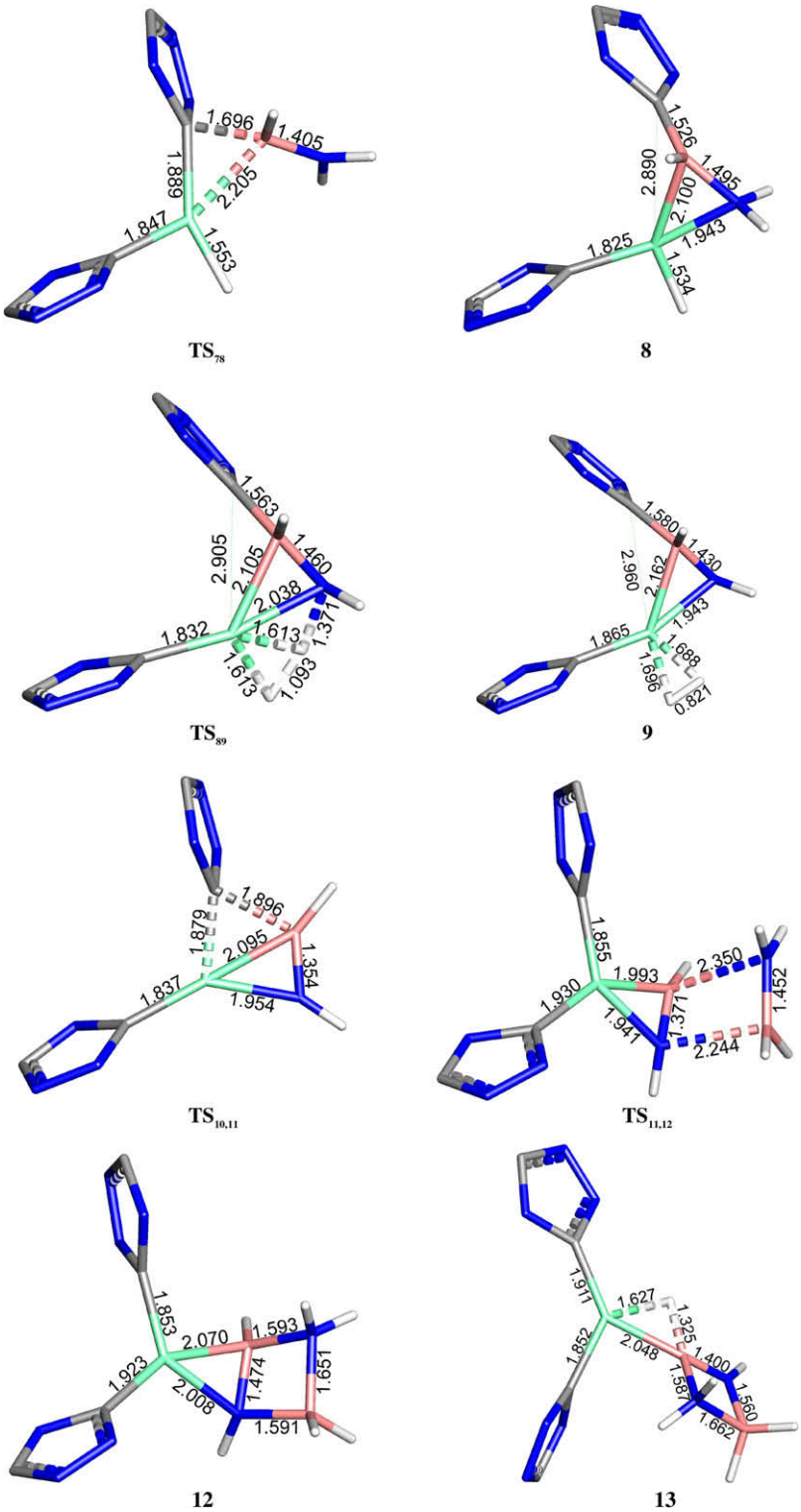


**Fig. 3.** Optimized geometric structures of complexes **8**, **9**, **12** and **13** and the transition states $\mathbf{TS_{78}}$ ($-195.6\ cm^{-1}$), $\mathbf{TS_{89}}$ ($-1160.2\ cm^{-1}$), $\mathbf{TS_{10,11}}$ ($-144.9\ cm^{-1}$) and $\mathbf{TS_{11,12}}$ ($-324.1\ cm^{-1}$). Bond lengths are in angstrom. The phenyl groups are not shown for clarity.

other stable intermediate **13** is formed with a new 3-center, 2-electron Ni–H–B bridging structure. Finally, the cyclic $N_2B_2H_6$ molecule can leave **13** and the catalyst **1** can be regenerated easily ($\Delta H$ = 11.4 kcal/mol).

With the formation of $N_2B_2H_6$, this catalytic reaction releases only 1.5 equiv. of $H_2$ from AB. This and other intermediate products generated through dehydrogenation will react further with the catalyst **1**, release more hydrogen from AB, and generate other $B_xN_yH_z$ molecules including borazine. Baker and coworkers observed further reactions between $B_xN_yH_z$ molecules after $H_2$ was released from AB [22]. Because of the large variety of these new complexes and the lack of additional experimental insight, further computational predictions for possible reactions are difficult.

**Table 4**
Deuterated relative gas-phase free energies of the rate determining steps **2** → **TS$_{23}$**, **4** → **TS$_{45}$**, **7** → **TS$_{71}$** and **7** → **TS$_{78}$** in the AB dehydrogenation mechanism.

| Steps | Relative enthalpies (kcal/mol) | | | |
|---|---|---|---|---|
| | $H_3N–BH_3$ | $H_3N–BD_3$ | $D_3N–BH_3$ | $D_3N–BD_3$ |
| $G^{\ddagger}$ (**TS$_{23}$**) − $G^{\circ}$ (**2**) | 11.33 | 11.35 | 12.47 | 12.49 |
| $G^{\ddagger}$ (**TS$_{45}$**) − $G^{\circ}$ (**4**) | 8.56 | 8.56 | 9.44 | 9.44 |
| $G^{\ddagger}$ (**TS$_{71}$**) − $G^{\circ}$ (**7**) | 8.52 | 8.47 | 8.49 | 8.44 |
| $G^{\ddagger}$ (**TS$_{78}$**) − $G^{\circ}$ (**7**) | 28.25 | 28.94 | 28.43 | 29.18 |

### 3.4. Analysis of the kinetic isotope effect

The kinetic isotope effects (KIEs) of 1.7, 2.3 and 3.0 for deuterations at boron, nitrogen and both of them in the dehydrogenation of AB catalyzed by $Ni(NHC)_2$ were obtained by Baker and coworkers. These results suggest that both N–H and B–H bonds are being broken in the rate determining steps. The calculated deuterated relative gas-phase free energies of the rate determining steps **2** → **TS$_{23}$**, **4** → **TS$_{45}$**, **7** → **TS$_{71}$** and **7** → **TS$_{78}$** at the optimized structures are given in Table 4. The atomic mass and nuclear spin of the deuterium atom were set as 2.0141018 and 1 (spin parallel). In the rate determining steps for the first $H_2$ release from AB, deuteration at boron does not change the barriers, but deuteration at nitrogen increases the free energy barriers of the **2** → **TS$_{23}$** and **4** → **TS$_{45}$** steps by 1.1 and 0.9 kcal/mol, respectively. These increases explain the observed larger KIE for deuteration at nitrogen. In the rate determining step for the second $H_2$ release, **7** → **TS$_{78}$**, deuteration at boron and nitrogen increases the free energy barriers by 0.7 and 0.2 kcal/mol, respectively. These increases explain the observed weaker KIE for deuteration at boron in the whole reaction. Since the experimental KIEs were obtained in the catalytic reaction for more than 2.5 equiv. of $H_2$ release, more than one rate determining steps is being sampled. Furthermore, a KIE for the deuteration at boron was not observed in the first 20 min (Fig. 2 in Ref. [17]). Therefore, our current results match well with the observed phenomena.

## 4. Conclusions

In summary, the mechanism for $Ni(NHC)_2$ catalyzed dehydrogenation of ammonia–borane was studied theoretically by using DFT method. This study proposes for the first time a possible mechanism for the second equivalent of $H_2$ release from AB for the first time. There are four main steps for the release of the first $H_2$ from AB (Scheme 1): (1) transfer of a proton from N to the unsaturated C in carbene, (2) transfer of H from this C to Ni, (3) transfer of H from B to Ni, and (4) release of $H_2$ and $H_2B–NH_2$ to regenerate the catalyst $Ni(NHC)_2$. For the release of second $H_2$ from AB (Scheme 2), our calculations predict six main steps: (1) the breaking of a 3-center, 2-electron Ni–H–B bridging structure with the formation of B–C and Ni–H bonds, (2) N–H bond activation with the formation of $H_2$, (3) $H_2$ release, (4) B–C bond activation for the regeneration of a Ni–C bond, (5) reaction with $H_2N–BH_2$ for the formation of $N_2B_2H_6$ and (6) $N_2B_2H_6$ release and regeneration of $Ni(NHC)_2$.

Our calculations also demonstrate that (1) the first $H_2$ release begins with proton transfer from nitrogen to the metal bound carbene carbon, instead of previously hypothesized B–H or N–H bond activation, (2) this new C–H bond is activated by the metal, transferring the H to Ni, then forming the $H_2$ molecule by transferring another H from B to Ni, rather than β-H transfer, (3) the second $H_2$ release from $H_2N–BH_2$ begins with the breaking of a 3-center, 2-electron Ni–H–B bridging structure with the assistance of the unsaturated carbene carbon atom to form a B–C bond, (4) a nearly rhombic $N_2B_2H_6$ molecule must be formed to help the regeneration of the catalyst $Ni(NHC)_2$, which also leads current catalytic mechanism releases only 1.5 equiv. of $H_2$ from AB. These points along the reaction pathways explain the importance of the NHC ligands in this catalytic process and yield lower energy barriers than mechanisms that begin with N–H or B–H activations catalyzed by the metal atoms. The predicted reaction mechanism which features unexpected ligand participation points the way to finding new catalysts with higher efficiency, as partial unsaturation of the M–L bond may be essential for low energy H atom transfers.

## Acknowledgments

This work was supported by the grants from NSF (CHE-0518074, CHE-0541587 and DMS-0216275) and The Welch Foundation (A0648).

## Appendix A. Supplementary material

Supplementary data associated with this article can be found, in the online version, at doi:10.1016/j.jorganchem.2009.04.018.

## References

[1] F.H. Stephens, R.T. Baker, M.H. Matus, D.J. Grant, D.A. Dixon, Angew. Chem., Int. Ed. 46 (2007) 746.
[2] J. Li, S.M. Kathmann, G.K. Schenter, M. Gutowski, J. Phys. Chem. C 111 (2007) 3294.
[3] M.E. Bluhm, M.G. Bradley, R. Butterick III, U. Kusari, L.G. Sneddon, J. Am. Chem. Soc. 128 (2006) 7748.
[4] Q.S. Li, J. Zhuang, S. Zhang, Chem. Phys. Lett. 404 (2005) 100.
[5] C.A. Morrison, M.M. Siddick, Angew. Chem., Int. Ed. 43 (2004) 4780.
[6] A. Feaver, S. Sepehri, P. Shamberger, A. Stowe, T. Autrey, G. Cao, J. Phys. Chem. B 111 (2007) 7469.
[7] A.C. Stowe, W.J. Shaw, J.C. Linehan, B. Schmid, T. Autrey, Phys. Chem. Chem. Phys. 9 (2007) 1831.
[8] C.R. Miranda, G.J. Ceder, Chem. Phys. 126 (2007) 184703.
[9] F.H. Stephens, V. Pons, R.T. Baker, Dalton Trans. (2007) 2613.
[10] X. Kang, Z. Fang, L. Kong, H. Cheng, X. Yao, G. Lu, P. Wang, Adv. Mater. 20 (2008) 2756.
[11] S.B. Kalidindi, U. Sanyal, B.R. Jagirdar, Phys. Chem. Chem. Phys. 10 (2008) 5870.
[12] M.C. Denney, V. Pons, T.J. Hebden, D.M. Heinekey, K.I. Goldberg, J. Am. Chem. Soc. 128 (2006) 12048.
[13] C.A. Jaska, K. Temple, A.J. Lough, I. Manners, J. Am. Chem. Soc. 125 (2003) 9424.
[14] Y. Chen, J.L. Fulton, J.C. Linehan, T. Autrey, J. Am. Chem. Soc. 127 (2005) 3254.
[15] T.J. Clark, C.A. Russell, I. Manners, J. Am. Chem. Soc. 128 (2006) 9582.
[16] Q. Xu, M. Chandra, J. Power Sources 163 (2006) 364.
[17] R.J. Keaton, J.M. Blacquiere, R.T. Baker, J. Am. Chem. Soc. 129 (2007) 1844.
[18] Y. Luo, K. Ohno, Organometallics 26 (2007) 3597.
[19] A. Paul, C.B. Musgrave, Angew. Chem., Int. Ed. 46 (2007) 8153.
[20] X. Yang, M.B. Hall, J. Am. Chem. Soc. 130 (2008) 1798.
[21] N. Blaquiere, S. Diallo-Garcia, S.I. Gorelsky, D.A. Black, K. Fagnou, J. Am. Chem. Soc. 130 (2008) 14034.
[22] V. Pons, R.T. Baker, N.K. Szymczak, D.J. Heldebrant, J.C. Linehan, M.H. Matus, D.J. Grant, D.A. Dixon, Chem. Commun. (2008) 6597.
[23] M. Dresselhaus, G. Crabtree, M. Buchanan (Eds.), Basic Energy Needs for the Hydrogen Economy: Basic Energy Sciences, Office of Science, US Department of Energy, Washington, DC, 2003. <http://www.sc.doe.gov/bes/hydrogen.pdf>.
[24] M.J. Frisch, G.W. Trucks, H.B. Schlegel, G.E. Scuseria, M.A. Robb, J.R. Cheeseman, J.A. Montgomery Jr., T. Vreven, K.N. Kudin, J.C. Burant, J.M. Millam, S.S. Iyengar, J. Tomasi, V. Barone, B. Mennucci, M. Cossi, G. Scalmani, N. Rega, G.A. Petersson, H. Nakatsuji, M. Hada, M. Ehara, K. Toyota, R. Fukuda, J. Hasegawa, M. Ishida, T. Nakajima, Y. Honda, O. Kitao, H. Nakai, M. Klene, X. Li, J.E. Knox, H.P. Hratchian, J.B. Cross, V. Bakken, C. Adamo, J. Jaramillo, R. Gomperts, R.E. Stratmann, O. Yazyev, A.J. Austin, R. Cammi, C. Pomelli, J.W. Ochterski, P.Y. Ayala, K. Morokuma, G.A. Voth, P. Salvador, J.J. Dannenberg, V.G. Zakrzewski, S. Dapprich, A.D. Daniels, M.C. Strain, O. Farkas, D. K. Malick, A.D. Rabuck, K. Raghavachari, J.B. Foresman, J.V. Ortiz, Q. Cui, A.G. Baboul, S. Clifford, J. Cioslowski, B.B. Stefanov, G. Liu, A. Liashenko, P. Piskorz, I. Komaromi, R.L. Martin, D.J. Fox, T. Keith, M.A. Al-Laham, C.Y. Peng, A. Nanayakkara, M. Challacombe, P.M.W. Gill, B. Johnson, W. Chen, M.W. Wong, C. Gonzalez, J.A. Pople, GAUSSIAN 03, Revision D.02, Gaussian Inc., Wallingford, CT, 2004.
[25] (a) J.P. Perdew, K. Burke, M. Ernzerhof, Phys. Rev. Lett. 77 (1996) 3865;
(b) J.P. Perdew, K. Burke, M. Ernzerhof, Phys. Rev. Lett. 78 (1997) 1396.
[26] A.D. Becke, J. Chem. Phys. 98 (1993) 5648.
[27] C. Lee, W. Yang, R.G. Parr, Phys. Rev. B 37 (1988) 785.
[28] (a) K. Burke, J.P. Perdew, Y. Wang, in: J.F. Dobson, G. Vignale, M.P. Das (Eds.), Electronic Density Functional Theory: Recent Progress and New Directions, Plenum, New York, 1998, pp. 81–111;
(b) J.P. Perdew, in: P. Ziesche, H. Eschrig (Eds.), Electronic Structure of Solids '91, Akademie Verlag, Berlin, 1991. p. 11;

(c) J.P. Perdew, J.A. Chevary, S.H. Vosko, K.A. Jackson, M.R. Pederson, D.J. Singh, C. Fiolhais, Phys. Rev. B 46 (1992) 6671;
(d) J.P. Perdew, J.A. Chevary, S.H. Vosko, K.A. Jackson, M.R. Pederson, D.J. Singh, C. Fiolhais, Phys. Rev. B 48 (1993) 4978;
(e) J.P. Perdew, K. Burke, Y. Wang, Phys. Rev. B 54 (1996) 16533.
[29] J.M. Tao, J.P. Perdew, V.N. Staroverov, G.E. Scuseria, Phys. Rev. Lett. 91 (2003) 146401.
[30] A.D. Boese, J.M.L. Martin, J. Chem. Phys. 121 (2004) 3405.
[31] (a) T.H. Dunning Jr., J. Chem. Phys. 90 (1989) 1007;
(b) D.E. Woon, T.H. Dunning Jr., J. Chem. Phys. 98 (1993) 1358.
[32] (a) JIMP2, version 0.091, a free program for visualizing and manipulating molecules M.B. Hall, R.F. Fenske, Inorg. Chem. 11 (1972) 768;
(b) J. Manson, C.E. Webster, M.B. Hall, Texas A&M University, College Station, Texas, 2006. <http://www.chem.tamu.edu/jimp2/index.html>.
[33] G.J. Kubas, Metal Dihydrogen and σ-Bond Complexes, Kluwer Academic/Plenum Publishers, New York, 2001.
[34] G. Parkin, Organometallics 25 (2006) 4744.